Cellular/Molecular

The Expression Pattern of a Cav3–Kv4 Complex Differentially Regulates Spike Output in Cerebellar Granule Cells

N. Colin Heath,[1] Arsalan P. Rizwan,[1] Jordan D.T. Engbers,[1] Dustin Anderson,[1] Gerald W. Zamponi,[2] and Ray W. Turner[1,2]

Departments of [1]Cell Biology and Anatomy and [2]Physiology and Pharmacology, Hotchkiss Brain Institute, University of Calgary, Calgary, Alberta, Canada T2N 4N1

The cerebellum receives sensory information by mossy fiber input from a multitude of sources that require differential signal processing. A compartmentalization of function begins with the segregation of mossy fibers across 10 distinct lobules over the rostrocaudal axis, with tactile receptor afferents prevalent in anterior lobules and vestibular input in caudal lobules. However, it is unclear how these unique signals might be differentially processed at the circuit level across the cerebellum. As granule cells receive mossy fiber input, they represent a key stage at which postsynaptic mechanisms could influence signal processing. Granule cells express an A-type current mediated by Kv4 potassium channels that modify the latency and frequency of spike output. The current study examined the potential for a Cav3 calcium–Kv4 channel complex to regulate the response of granule cells to mossy fiber input in lobules 2 and 9 of the rat cerebellum. Similar A-type currents were recorded in both regions, but the Cav3 calcium current was expressed at a substantially higher density in lobule 9 cells, acting to increase A-type current availability through its influence on Kv4 voltage for inactivation. The difference in excitability imparted by Cav3–Kv4 interactions proves to allow lobule 2 granule cells to respond more effectively to tactile stimulus-like burst input and lobule 9 cells to slow shifts in input frequency characteristic of vestibular input. The expression pattern of Cav3 channels and its control of Kv4 availability thus provides a novel means of processing widely different forms of sensory input across cerebellar lobules.

Key words: **A-type potassium; Cav3; cerebellum; granule cell; Kv4; T-type calcium**

Introduction

The cerebellum processes sensory input that ranges from brief tactile sensation communicated through the somatosensory system to slow shifts in head position signaled by vestibular organs. In each case, mossy fiber (MF) inputs terminate in a granule cell layer to begin signal processing by circuitry that is conserved across all cerebellar regions. How signals that convey such widely disparate forms of information can be differentially processed is only beginning to be understood. One strategy to compartmentalize signal processing is apparent in the projection of MF afferents across 10 distinct lobules over the cerebellar rostrocaudal axis. In general, in the midline vermis region, MF inputs and outputs related to limb afferents are centered in lobules 1–5, cognitive and oculomotor functions in lobules 6–8, and vestibular function in lobules 9 and 10 (Armstrong et al., 1997; Sillitoe and Joyner, 2007; Glickstein et al., 2011; Valle et al., 2012). Differential signal processing can also incorporate the pattern of presynaptic MF spike input conveying different sensory stimuli (Bengtsson and Jörntell, 2009; Chadderton et al., 2014), convergence of sensory inputs (Ekerot and Jörntell, 2008; Chadderton et al., 2014), synaptic plasticity (D'Angelo and De Zeeuw, 2009), or the new circuit elements [i.e., unipolar brush cells (UBCs); Mugnaini et al., 2011; Kim et al., 2012]. The importance of postsynaptic processing of sensory inputs that shape granule cell firing has also been recognized (D'Angelo and De Zeeuw, 2009), although the ion channels responsible for modulating spike output are not fully understood.

One of the most prominent currents expressed by granule cells is an A-type potassium current (I_A) mediated by Kv4 channels (Cull-Candy et al., 1989; Serôdio and Rudy, 1998; Maffie and Rudy, 2008). Kv4 channels are distinct among A-type channels in forming a complex with members of the calcium-sensing potassium channel interacting proteins (KChIPs; An et al., 2000; Jerng et al., 2005; Norris et al., 2010). An association of the Kv4 com-

Received March 12, 2014; revised May 15, 2014; accepted May 20, 2014.

Author contributions: N.C.H., A.P.R., J.D.T.E., D.A., and R.W.T. designed research; N.C.H., A.P.R., J.D.T.E., and D.A. performed research; J.D.T.E. and G.W.Z. contributed unpublished reagents/analytic tools; N.C.H., A.P.R., J.D.T.E., D.A., G.W.Z., and R.W.T. analyzed data; N.C.H., A.P.R., J.D.T.E., and R.W.T. wrote the paper.

This work was supported by a grant from the Canadian Institutes of Health Research (CIHR; to R.W.T. and G.W.Z.), studentships through the Alberta Heritage Foundation for Medical Research (D.A., J.D.T.E.), a T. Chen Fong award (D.A., J.D.T.E.), the Killam Foundation (D.A., J.D.T.E.), and a CIHR-Canada Graduate Scholarship (CGS) PhD studentship (J.D.T.E.). G.W.Z. is an AI-HS Scientist and Canada Research Chair, and R.W.T. is an Alberta Innovates-Health Solutions (AI-HS) Scientist. We gratefully acknowledge S. Hameed, M. Kruskic, and L. Chen for expert technical assistance.

The authors declare no competing financial interests.

Correspondence should be addressed to Ray W. Turner, Hotchkiss Brain Institute, HRIC 1AA14, University of Calgary, 3330 Hospital Drive, N.W., Calgary, AB, Canada T2N 4N1. E-mail: rwturner@ucalgary.ca.

DOI:10.1523/JNEUROSCI.0981-14.2014

 0270-6474/14/348800-13$15.00/0

plex with Cav3 T-type calcium channels and KChIP3 was also shown to invoke a calcium-sensitive increase in I_A that modifies spike output in cerebellar stellate cells (Molineux et al., 2005; Anderson et al., 2010a, 2013). It is important, then, that both Cav3 calcium (Talley et al., 1999) and Kv4 potassium channel isoforms (Serôdio and Rudy, 1998; Amarillo et al., 2008) exhibit pronounced gradients of expression in granule cells over cerebellar lobules that could help define signal processing.

The current study tested the hypothesis that cerebellar granule cell excitability is differentially regulated across cerebellar lobules by the expression pattern of members of the Cav3–Kv4 channel complex. We find that Cav3 calcium current (I_T) and its regulation of I_A are present in lobule 9 granule cells but nearly absent in lobule 2 granule cells, indicating that the expression pattern of Cav3 channels can govern the functional activity of the Cav3–Kv4 complex. The Cav3–Kv4 complex also differentially modifies the gain of firing in lobule 2 versus lobule 9 granule cells that serves to shape the response to MF input patterns inherent to rostral and caudal cerebellar lobules.

Materials and Methods

Animal care and slice preparation. Sprague Dawley rats were obtained weekly from Charles River and maintained according to the guidelines of the Canadian Council for Animal Care. All chemicals were obtained from Sigma-Aldrich unless otherwise noted. Transverse cerebellar slices (250–300 μm) were prepared from the midline vermis region of male rats at postnatal days 19–23 (P19–P23) using established procedures (Anderson et al., 2010a). Briefly, animals were anesthetized with isoflurane until they were unresponsive to tail pinch, and the cerebellum was dissected out in artificial CSF (aCSF) composed of (in mM) 125 NaCl, 3.25 KCl, 1.5 $CaCl_2$, 1.5 $MgCl_2$, 25 $NaHCO_3$, and 25 D-glucose preoxygenated by carbogen (95% O_2, 5% CO_2) gas. Tissue slices were cut by vibratome, and the temperature was elevated to 34°C for 60 min before storing in carbogen-gassed aCSF at room temperature. Recordings were obtained from slices maintained as a submerged preparation at 32–34°C on the stage of Axioskop II (Zeiss) or BH-50/BX51W1 (Olympus) microscopes equipped with differential interference contrast optics and infrared light transmission.

Electrophysiology. Whole-cell patch clamp recordings were obtained using Multiclamp 700B amplifiers and pClamp software (Molecular Devices). Dynamic-clamp recordings were obtained using a BNC-2090 Digital/Analog converter (National Instruments) and a computer running 64-bit OpenSuSE 11.1 with a real-time kernel and the real-time experimental interface (Dorval et al., 2001), as described previously (Anderson et al., 2013). Electrodes had a resistance of 6–8 MΩ and an access resistance of 8–15 MΩ, with cells rejected for any drift in access resistance of >20%. A calculated junction potential of −10 mV was subtracted from current-clamp recordings. Less than 10 pA of bias current was applied to maintain the resting potential of granule cells at approximately −90 mV. During delivery of simulated EPSCs (simEPSCs), negative bias current was applied to maintain the resting membrane potential at approximately −72 mV. Granule cells exhibit a high input resistance (R_i) that leads to substantial jitter in the latency of first spikes evoked by square current injection that prevented quantification of first-spike latency.

We found that current-clamp recordings conducted using a K-gluconate-based electrolyte buffered with 0.1 EGTA exhibited progressive increases in resting excitability. Therefore, we used an internal electrolyte established to invoke less change in intrinsic excitability (in mM): 126 K-gluconate, 4 NaCl, 5 HEPES, 1 $MgSO_4$, 0.15 BAPTA, and 0.05 $CaCl_2$, pH 7.25 via KOH (Gall et al., 2005). For both current- and voltage-clamp recordings, 5 mM di-Tris-creatine phosphate, 2 mM Tris-ATP, and 0.5 mM Na-GTP were added from fresh, frozen stock each day. In support of this, we found no significant change in the mean gain of spike firing over a period of 10 min with this solution [gain of lobule 9 cells: 0 min, 6.1 ± 0.69 Hz/pA; 10 min, 5.9 ± 0.28 Hz/pA; $n = 3$]. Voltage-clamp recordings of I_A used an internal solution (in mM: 140 KCl, 0.1 EGTA, 10 HEPES, and 2.5 $MgCl_2$, pH adjusted to 7.3 with KOH) and external aCSF [in mM: 0.0001 TTX, 5 tetraethylammonium chloride (TEA), and 2 CsCl]. I_A was recorded in the presence of Cav3 calcium currents to preserve the Cav3–Kv4 inaction, with no external Cd^{2+} to block high-voltage-activated (HVA) calcium currents to avoid effects on Kv4 activation voltage (see Fig. 3*A*; Song et al., 1998). Voltage-clamp recordings of I_T used an internal solution of (in mM) 100 CsCl, 10 EGTA, 10 HEPES, and 3 $MgCl_2$ and the same set of external blockers as for I_A recordings, with the addition of 5 mM 4-aminopyridine (4-AP) and 30 μM Cd^{2+} to block HVA calcium channels, including R-type calcium channels (Engbers et al., 2012). Except where noted, synaptic transmission was blocked in all recordings with bath-applied AP-5 (25 μM), DNQX (10 μM; Tocris), CGP-55845 (1 μM; Tocris), and picrotoxin (50 μM). A mouse monoclonal Pan-KChIP antibody (catalog #73-006 RRID: AB_2132595; UC Davis/NIH NeuroMab Facility) was included in the patch electrode at 1:100 dilution in specific experiments. For control tests, PanKChIP antibody was denatured by heat inactivation for 1 h in boiling water.

Data analysis. Data analyses were performed using a combination of pCLAMP 10, Origin 8.0 (OriginLab), and custom Matlab scripts. Steady-state activation and inactivation curves were fit with Boltzmann functions according to following:

$$h_\infty = \frac{1}{1 + e^{-(V - V_h)/k}}, \quad (1)$$

where V is the membrane voltage, V_h is the half-activation/-inactivation voltage, and k is the slope factor.

Results

The activity of granule cells was assessed in sagittal tissue slices in the midline vermal region and in cells positioned within the upper third of the granule cell layer (proximal to the Purkinje cell layer). Recordings were focused in lobules 2 and 9 to examine activity at representative extremes of the reported gradients for Kv4 and Cav3 channel isoforms (Talley et al., 1999). Granule cell recordings were accepted if spike height attained a peak value of +10 mV or greater, an ability to reach spike threshold within 15–30 pA current injection, and little or no spike accommodation or loss of spike height during current pulse injections. Baseline comparisons with no bias current injection detected no significant difference between lobule 2 and 9 cells in terms of membrane capacitance, resting membrane potential, or spike threshold (data not shown). Golgi cell recordings were distinguished from granule cells on the basis of visual inspection (20 μm diameter for Golgi cells vs 7–8 μm for granule cells), a larger membrane capacitance (40–50 pF for Golgi cells vs 4–9 pF for granule cells), and marked spike accommodation during current pulse injection ($n = 3$; Locatelli et al., 2013). UBCs were distinguished by a lower input resistance (R_i; 750–850 MΩ for UBCs vs >1 GΩ for granule cells) and higher membrane capacitance (10–12 pF for UBCs vs 5–8 pF for granule cells) (D'Angelo et al., 1998; Diana et al., 2007; Locatelli et al., 2013).

Cav3 (T-type) calcium channels are differentially expressed in granule cells

The reported expression pattern of calcium channels in granule cells has differed according to preparation and recording conditions. A number of HVA calcium currents were reported for granule cells dissociated from P2–P5 rats and maintained in culture (Randall and Tsien, 1995; Tottene et al., 1996, 2000), including studies delineating the properties of R-type (Cav2.3) calcium channels (Randall and Tsien, 1997; Tottene et al., 2000). HVA calcium channels also contribute to granule cell activity in intact tissue but exhibit a developmental reduction in functional expression by approximately P20 (Rossi et al., 1994; D'Angelo et al.,

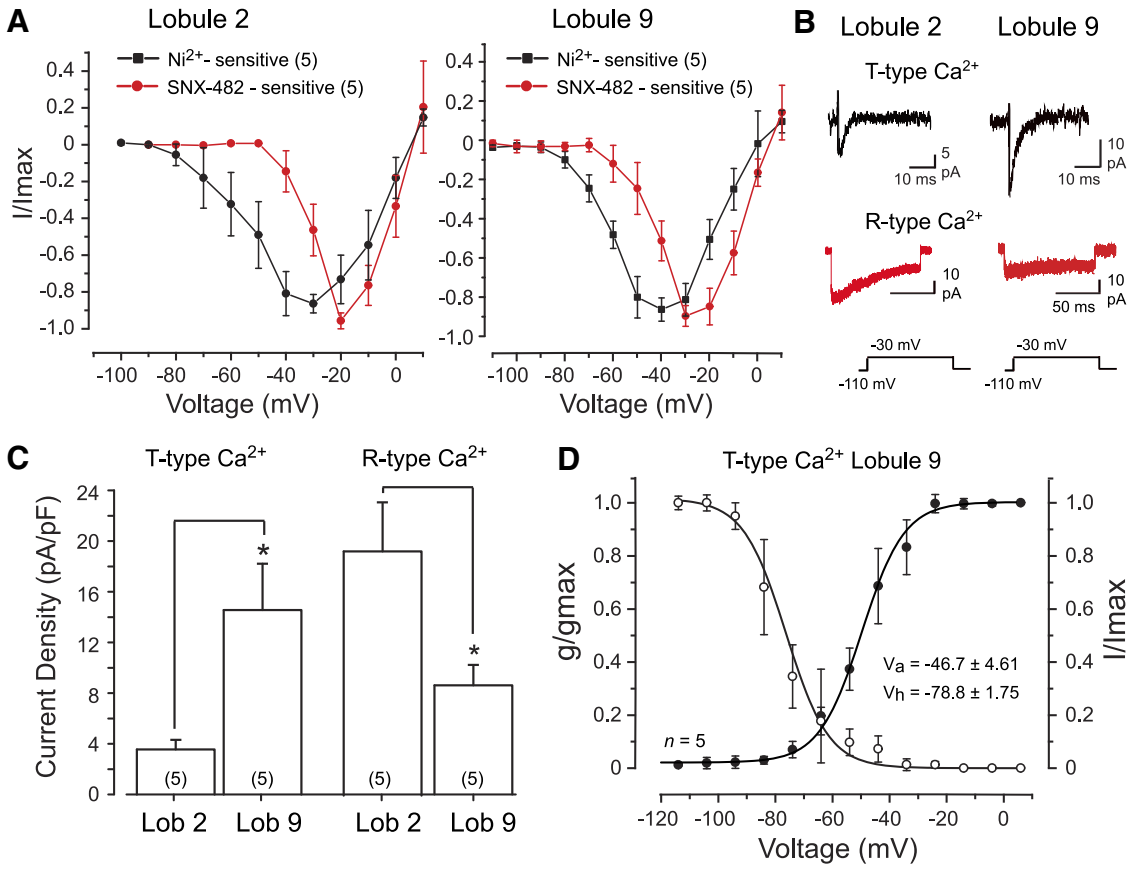

Figure 1. Cerebellar granule cells express Cav3 calcium current. ***A***, Comparisons between the mean *I–V* plots of calcium current in lobule 2 and 9 granule cells. Cav3 current was identified as the component sensitive to block by 300 μM Ni^{2+} (in the presence of 30 μM Cd^{2+}) and R-type current as that blocked by 200 nM SNX-482 (in the absence of Cd^{2+}). ***B***, Representative T-type and R-type calcium currents in lobule 2 and lobule 9 granule cells. ***C***, Bar plots of the mean density of T-type and R-type calcium currents isolated as in ***A*** and ***B*** for lobule 2 and 9 granule cells for a step from −110 to −30 mV. ***D***, Superimposed mean conductance- and voltage-inactivation plots for T-type calcium current in lobule 9 granule cells. Sample numbers for mean values are shown in parentheses. *$p < 0.05$, Student's paired *t* test.

1997, 1998). By comparison, <1% of cultured granule cells were reported to express calcium currents consistent with T-type channels (Randall and Tsien, 1995). On the other hand, evidence for Cav3 channel expression was obtained through *in situ* hybridization, with strong labeling for Cav3.1 mRNA in granule cells of lobules 6–10 but virtually no expression in granule cells of rostral lobules (Talley et al., 1999). By comparison, Cav3.3 mRNA was detected at a lower and relatively uniform level in granule cells across all lobules (Talley et al., 1999). We thus examined the ability to record low-voltage-activated (LVA) Cav3 calcium currents in granule cells of tissue slices prepared from P19–P24 rats.

T-type calcium current was isolated by perfusing 30 μM Cd^{2+} to block HVA and R-type calcium channels (Ellinor et al., 1993; Zhang et al., 1993; Randall and Tsien, 1995, 1997; Engbers et al., 2012) and also identified as the inward current sensitive to block by 300 μM Ni^{2+}, a concentration within the IC_{50} for Cav3.1 and Cav3.3 isoforms (Lee et al., 1999). The bathing medium also contained blockers of Kv4 potassium (5 mM 4-AP), sodium (1 μM TTX), hyperpolarization-activated cyclic nucleotide-gated (HCN) (2 mM CsCl), KCa2.x (100 nM apamin), KCa1.1 channels (5 mM TEA), and excitatory and inhibitory synaptic blockers. Whole-cell recordings were used to apply a holding potential of −110 mV and step commands to +10 mV in 10 mV steps, with 300 μM Ni^{2+} applied by bath perfusion. Under these conditions, a Ni^{2+}-sensitive LVA transient inward current could be identified in both lobule 2 and lobule 9 granule cells. The current activated near approximately −75 mV and peaked at approximately −30 mV in both lobules on current–voltage (*I–V*) plots (Fig. 1*A*) and was fast activating and inactivating (Fig. 1*B*). As characteristically found, reversal for the isolated T-Ca^{2+} current was in the range of 0–20 mV on *I–V* plots (Fig. 1*A*; Iftinca et al., 2006). The fast transient current was significantly smaller in amplitude in lobule 2 cells (range, 5.5–19.5 pA at −30 mV), with approximately four times greater current density in lobule 9 granule cells (Fig. 1*C*).

Given reports of R-type calcium current in granule cells and the sensitivity of both T-type and R-type calcium channels to Ni^{2+} (Randall and Tsien, 1995; Tottene et al., 1996; Zamponi et al., 1996), we also identified the component of calcium current that could be blocked by the Cav2.3 R-type channel blocker SNX-482. These tests used a similar bath perfusate as above but excluded Cd^{2+} to retain HVA calcium currents. R-type currents were then identified by applying 200 nM SNX-482 from a local pressure electrode that also contained all bath-applied blockers. SNX-482-sensitive currents showed initial activation on *I–V* plots at approximately −50 mV or above and peaked at approximately −20 mV in both lobule 2 and 9 granule cells (Fig. 1*A*). Currents blocked by SNX-482 were also fast activating but very slow inactivating (Fig. 1*B*), as reported previously for R-type current in granule cells (Tottene et al., 2000). Finally, the density of SNX-482-sensitive current was significantly higher in lobule 2 cells compared with lobule 9 cells (Fig. 1*C*). Calcium currents

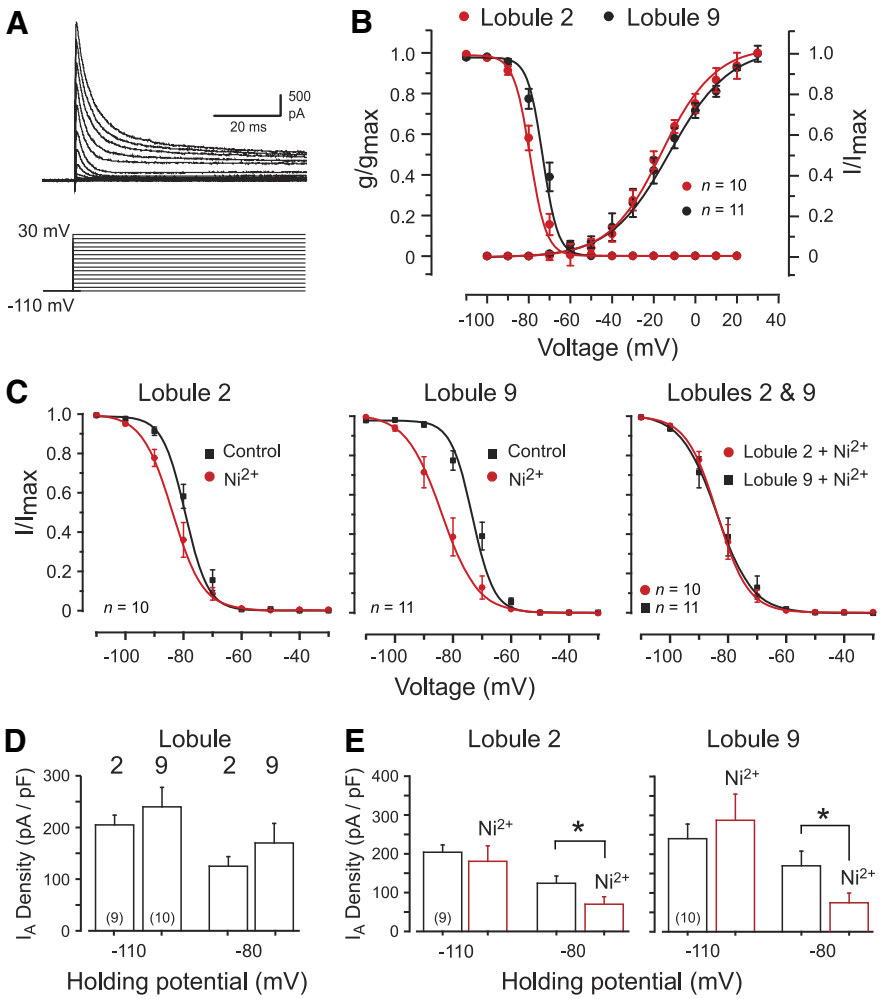

Figure 2. Biophysical properties of A-type current in granule cells of lobules 2 and 9. All recordings were conducted in the absence of calcium channel blockers unless indicated. ***A***, Kv4 current (I_A) evoked in a lobule 9 granule cell over the indicated potentials. ***B***, Mean conductance and voltage-inactivation plots for I_A in lobule 2 and 9 granule cells superimposed for comparison. ***C***, Voltage-inactivation plots for I_A in lobule 2 and 9 granule cells before and after 300 μM Ni^{2+} to block the Cav3–Kv4 interaction. Ni^{2+} produces a greater leftward shift of V_h in lobule 9 cells (left and middle), with a common V_h in either lobule once Cav3 current is blocked (right). ***D***, Bar plots of I_A density evoked by a step to −30 mV from two different holding potentials that are beyond (−110 mV) or within (−80 mV) the range of Ni^{2+}-sensitive shifts in I_A V_h. ***E***, Bar plots of I_A density evoked by a step to −30 mV from either −110 or −80 mV before and after 300 μM Ni^{2+}. *$p < 0.05$ (Student's paired t test).

blocked by SNX-482 were thus distinct from those of Ni^{2+}-sensitive calcium currents in terms of voltage sensitivity and rate of inactivation, and they were expressed with a current density opposite to that found for putative T-type calcium currents between lobule 2 and 9 granule cells. Although not all R-type calcium channel isoforms are SNX-482 sensitive (Tottene et al., 2000), these data are consistent with the expression of both Cav3 and Cav2.3 calcium channels. Moreover, the higher density of transient calcium current in lobule 9 granule cells coincides with the higher level of Cav3.1 mRNA reported in caudal cerebellar lobules (Talley et al., 1999). We thus consider the Ni^{2+}-sensitive transient calcium current as corresponding to primarily Cav3.1 channels in lobule 9 and Cav3.3 in lobule 2 granule cells (Talley et al., 1999).

In the course of comparing Cav3 channel properties between lobules, we found a very similar voltage for initial detection of Cav3 current on *I–V* plots for both lobule 2 and 9 cells (Fig. 1*A*). However, the very low density of Cav3 current in lobule 2 cells often prevented detailed characterization of conductance or inactivation properties. We thus focused on Cav3 currents recorded in lobule 9 to examine voltage-dependent properties. Calculating the mean voltage-conductance plot for Cav3 current in lobule 9 cells revealed a half-activation voltage (V_a) of −46.7 ± 4.61 mV with slope factor k = 8.7 ± 1.10 (n = 5; Fig. 1*D*). The half-inactivation voltage (V_h) was calculated using a test potential to −30 mV that followed the series of activation steps from −110 to +30 mV (1 s duration). Cav3 current in lobule 9 granule cells had a V_h of −78.8 ± 1.75 mV with slope factor k = 9.6 ± 3.59 (n = 5; Fig. 1*D*). These data indicate that the primary difference in properties of Cav3 calcium current that we could detect between lobule 2 and 9 granule cells was an approximate four times higher density in lobule 9 cells.

Kv4-mediated A-type potassium current

The biophysical properties of I_A in granule cells were assessed using whole-cell recordings and the same voltage step protocol as described above for Cav3 currents. Granule cells are known to lack apamin sensitivity but do exhibit a charybdotoxin-sensitive and low TEA (1 mM)-sensitive fast AHP (D'Angelo et al., 1998), indicating the expression of KCa1.1 but not KCa2.x channels. Thus, to isolate Kv4 current, we perfused TEA (5 mM), CsCl (2 mM), and TTX (1 μM) to block KCa1.1, HCN, and sodium channels, respectively, but excluded 4-AP to preserve Kv4 currents. We also excluded Cd^{2+} from the external medium given nonspecific effects on Kv4 activation voltage (see Fig. 3*A*; Song et al., 1998; Jerng et al., 2004). It has been shown through *in situ* hybridization and immunocytochemistry that the Kv4.2 and Kv4.3 isoforms are expressed in opposite gradients across cerebellar lobules, with a higher density of Kv4.3 in caudal lobules and higher levels of Kv4.2 in rostral lobules (Serôdio and Rudy, 1998; Amarillo et al., 2008). It is also known that the kinetics of Kv4 can be shaped by various factors, including the auxiliary KChIP subunits and dipeptidyl peptidase proteins (DPPs; Amarillo et al., 2008; Maffie and Rudy, 2008; Nadin and Pfaffinger, 2010, 2013; Kunjilwar et al., 2013). Thus, there are several factors that might predicate a difference in the baseline properties of Kv4 current between cerebellar lobules independent of an influence by a Cav3–Kv4 complex.

Under our conditions, voltage steps from −110 to +30 mV consistently evoked a net outward fast-activating current (I_A) of up to 4.8 nA in both lobule 2 and 9 granule cells (Fig. 2*A*). The current was fast inactivating but, as reported previously, did not show complete inactivation at higher voltage steps (Amarillo et al., 2008). The voltage dependence of I_A activation was equivalent in cells from lobules 2 and 9, initially detected on conductance plots in the range of −70 mV (Fig. 2*B*), with no significant difference in slope factors for voltage-activation plots (Table 1). No significant differences were detected in the slope factors for

Table 1. Properties of lobule 2 versus lobule 9 granule cell A-type current

	Lobule 2	Lobule 9
V_h (mV)	−77.7 ± 1.47 (10)*	−72.7 ± 1.47 (11)
k (inactivation)	3.8 ± 0.22 (10)	4.2 ± 0.18 (11)
V_a (mV)	−1.6 ± 4.59 (10)	6.3 ± 6.9 (11)
k (activation)	24.2 ± 5.45 (10)	22.4 ± 3.65 (8)
$t_{1/2}$ inactivation (ms)	2.0 ± 0.27 (6)	1.8 ± 0.17 (8)
τ recovery from inactivation (ms)	18.6 ± 3.85 (5)	16.9 ± 1.98 (8)

V_h, Half-inactivation potential; V_a half-activation potential. *$p < 0.05$, Student's unpaired t test.

voltage-inactivation plots, in the time for half-inactivation ($t_{1/2}$), or in the time constant for recovery from inactivation (for steps from −80 to −30 mV for 10–60 ms and test potential of −30 mV; Table 1). However, the half-inactivation voltage of I_A (V_h) was significantly right-shifted by ~5 mV in lobule 9 granule cells compared with lobule 2 cells ($p < 0.05$; Fig. 2*B*, Table 1).

In cerebellar stellate cells, it was shown that interfering with the Cav3–Kv4 complex by applying Cav3 channel blockers (Ni^{2+}, mibefradil) or lowering extracellular calcium concentration reduced I_A availability by left-shifting V_h by approximately −10 mV (Anderson et al., 2010a, 2013). It has been suggested that R-type calcium influx can couple to Kv4 channels in dendritic spines of hippocampal CA1 neurons (Wang et al., 2014). This is important in that blocking R-type channels with Ni^{2+} application might account for any detected change in I_A properties. However, in our experience, none of the HVA calcium channel subtypes modulated the Kv4 complex even when overexpressed in tsA-201 cells (Anderson et al., 2010b). Thus, applying the R-type channel blocker SNX-482 (600 nM) on Cav2.3 channels coexpressed with Kv4.2, KChIP3, and DPP10 cDNA in tsA-201 cells had no effect on the V_h of I_A (control V_h, −66.8 ± 0.8 mV; test V_h, −67.6 ± 1.5 mV; $n = 7$; $p > 0.05$). Similarly, pressure ejection of SNX-482 (200 nM) onto granule cells in lobule 9 produced no significant effect on I_A V_h (control V_h, −67.8 ± 1.74 mV; SNX-482, −67.9 ± 1.68 mV; $n = 3$; $p > 0.05$). Therefore, any effects of Ni^{2+} application on I_A were taken to indicate a block of Cav3-mediated calcium influx.

To test the role of Cav3-mediated calcium influx on I_A V_h in granule cells, we applied 300 μM Ni^{2+}, a concentration confirmed to have no effect on Kv4 current expressed in isolation in an expression system (Fig. 3*B*). After application of Ni^{2+}, lobule 2 granule cells exhibited no significant change in I_A V_h from −77.7 ± 1.48 to −82.7 ± 1.77 mV ($n = 10$; $p > 0.05$; Fig. 2*C*). By comparison, Ni^{2+} perfusion produced a significant leftward shift in I_A V_h in lobule 9 cells from −72.3 ± 1.47 to −82.8 ± 2.53 mV ($n = 11$; $p < 0.001$; Fig. 2*C*). Moreover, after Ni^{2+} perfusion, the values of I_A V_h in lobule 2 and 9 granule cells were not significantly different ($p > 0.05$; Fig. 2*C*). By comparison, Ni^{2+} produced no significant shift in slope factors (k) for the voltage-inactivation relationships for either lobule 2 or 9 cells (lobule 9 control, 4.16 ± 0.18; Ni^{2+}, 4.03 ± 0.15; $n = 11$; $p > 0.05$). To further test the use of Ni^{2+} as a Cav3 channel blocker, we repeated these experiments in lobule 9 cells using 1 μM mibefradil and found an equivalent leftward shift in I_A V_h (−75.2 ± 2.1 to −84.9 ± 1.5 mV; $n = 5$; $p < 0.05$). These data are all consistent with a Cav3 channel-mediated rightward shift in I_A V_h primarily in lobule 9 granule cells.

To further examine the influence of the Cav3–Kv4 complex on I_A availability, comparisons were made of I_A current density from different holding potentials before and after Ni^{2+} application. The reason for this comparison is that shifts in the V_h of I_A determined in Figure 2*C* predict that there should be no change

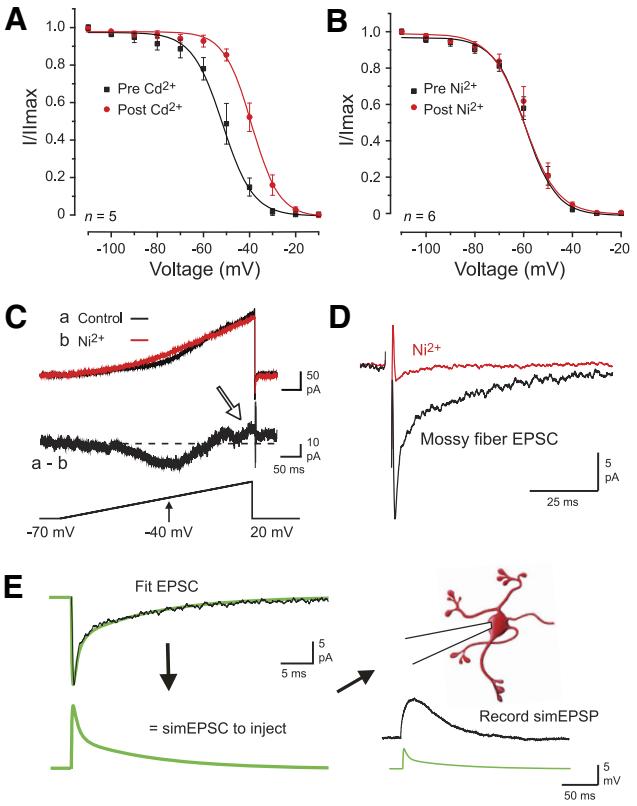

Figure 3. Pharmacology governing the study of a Cav3–Kv4 interaction in granule cells. ***A***, ***B***, The voltage-inactivation plot for Kv4.2 channels expressed in tsA-201 cells is shifted by 30 μM Cd^{2+} but not 300 μM Ni^{2+}. ***C***, Calcium and potassium currents evoked by a voltage ramp command in a lobule 9 granule cell in the presence of internal 4-AP (2 mM) and external TTX (1 μM) and CsCl (2 mM) to block Kv4, sodium, and HCN channels. Perfusing 300 μM Ni^{2+} reveals a LVA calcium current and calcium-activated potassium current (a, b; presumed KCa1.1, arrow). ***D***, Superimposed MF-evoked EPSCs reveal that 300 μM Ni^{2+} blocks the EPSC, preventing pharmacological block of Cav3 channels during MF-evoked responses. ***E***, Method of constructing simEPSCs to evoke postsynaptic simEPSPs. MF-evoked EPSCs were first recorded in granule cells, and the recorded response fit with exponentials to generate a simEPSC for injection into granule cell somata. The drawing of the cell was modified from Arenz et al. (2009).

in I_A availability when tested from −110 mV (for a step to −30 mV). On the other hand, the voltage range over which Ni^{2+} induced a shift in the inactivation profiles predicts that a similar test conducted from a holding potential of −80 mV should detect an effective calcium-dependent change in I_A availability. When this test was applied from a holding potential of −110 mV, we found no significant difference in I_A amplitude before and after Ni^{2+} application in cells of either lobule (lobule 2, $p > 0.05$; lobule 9, $n = 10$; $p > 0.05$; Fig. 2*D*,*E*). In contrast, we detected a significant decrease in I_A amplitude in both lobules during Ni^{2+} perfusion when tested from a holding potential of −80 mV (lobule 2, $p < 0.01$; lobule 9, $p < 0.01$; Fig. 2*E*). Therefore, an influence of the Cav3–Kv4 complex could be detected in cells in both lobules, but with a far greater effect on the voltage for inactivation in lobule 9 granule cells.

Kv4 regulation of spike firing in granule cells

I_A is known to control the interspike interval in many cells, including cerebellar granule cells (Connor and Stevens, 1971; D'Angelo et al., 1998; Liss et al., 2001; Yuan et al., 2005; Carrasquillo et al., 2012; Anderson et al., 2013). A calcium-dependent modulation of A-type current such as that provided by a Cav3–Kv4 complex could then regulate granule cell input–output

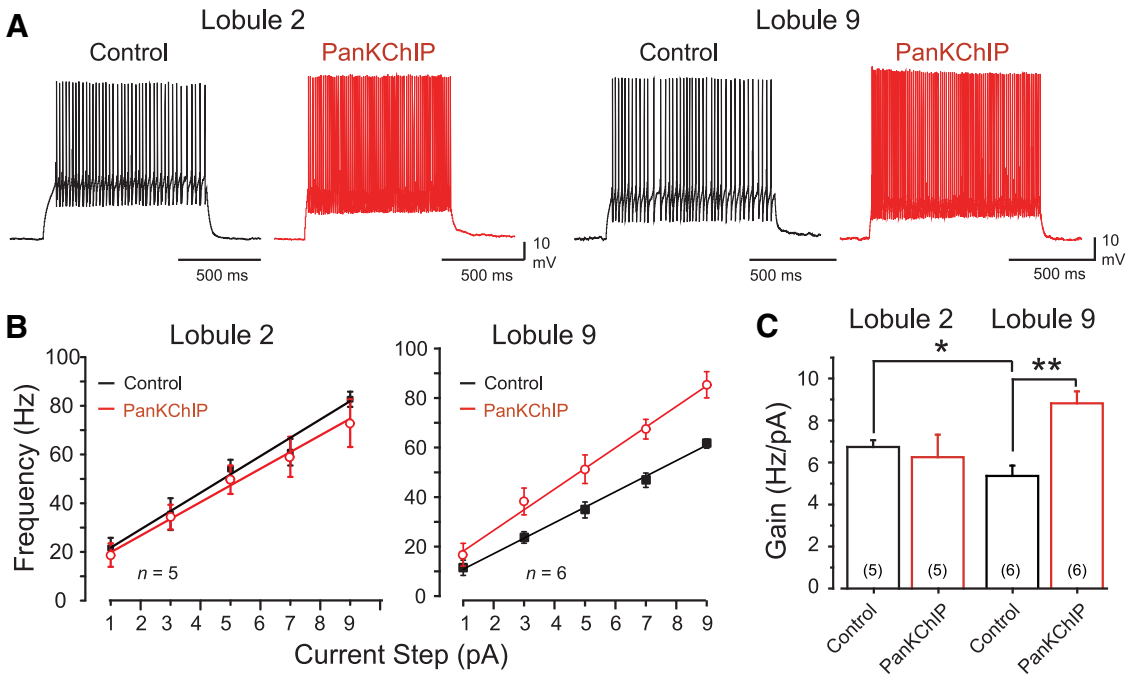

Figure 4. Internal block of the Cav3–Kv4 complex selectively increases firing rate gain in lobule 9 granule cells. ***A***, Representative recordings of current-evoked firing (1 s) in separate granule cells in the absence or presence of a PanKChIP antibody in the electrolyte (1:100 dilution) to block the Cav3–Kv4 interaction. ***B***, ***C***, Average current–frequency plots (***B***) and mean gain of firing (***C***) of granule cells in response to stimuli as shown in ***A*** in the absence or presence of the internal PanKChIP antibody. Interfering with the Cav3–Kv4 interaction reveals an increase in firing rate gain in lobule 9 but not lobule 2 granule cells. Sample numbers for mean values in bar plots are shown in parentheses. *$p < 0.05$; **$p < 0.01$, Student's unpaired *t* test.

relationships. Therefore, we tested the hypothesis that the distribution and activity of the Cav3–Kv4 complex differentially regulates spike firing between lobules 2 and 9. Here we measured the gain of firing by constructing frequency–current (*F–I*) plots of spike output and tested the effects of modulating Cav3–Kv4 complex function.

Internal block of Cav3–Kv4 complex function increases the gain of lobule 9 cells

When studying I_A under voltage clamp, we were able to reduce Cav3 calcium current by perfusing a low concentration of Ni^{2+} and could isolate I_A because we could pharmacologically eliminate calcium-dependent potassium channels. However, there were fewer options to isolate the Cav3–Kv4 complex for analysis under current-clamp conditions without affecting other calcium-dependent potassium channels that could be activated by calcium influx (Fig. 3*C*). Therefore, it was important to disrupt the interaction between Cav3 and Kv4 without altering calcium entry via Cav3 channels. There are currently no known external blockers of the Cav3–Kv4 complex. However, it has been shown that antibodies that target the KChIP3 calcium sensor subunit can be highly effective at interfering with the Cav3–Kv4 interaction (Anderson et al., 2010a). Thus, monoclonal antibodies against either KChIP3 or a PanKChIP antibody infused into cerebellar stellate cells by dialysis through the electrode rapidly promoted a leftward shift of Kv4 V_h (Anderson et al., 2010a). We repeated these tests on lobule 9 granule cells and found that infusion of the PanKChIP antibody (1:100 dilution) again produced a significant leftward shift in I_A V_h (control V_h, -71.9 ± 1.28 mV; test V_h, -78.9 ± 2.83 mV; $n = 5$; $p < 0.05$), a value not significantly different from that invoked by either Ni^{2+} ($n = 11$; $p > 0.05$) or mibefradil ($n = 5$; $p > 0.05$). By comparison, infusion of a denatured PanKChIP antibody had no significant effect on I_A V_h in lobule 9 granule cells (control V_h, -71.9 ± 1.28 mV; test V_h, -74.0 ± 0.90 mV; $n = 5$; $p > 0.05$). Moreover, including the PanKChIP antibody in the electrolyte occluded any additional shift in V_h of lobule 9 cells with subsequent perfusion of 300 μM Ni^{2+} (PanKChIP V_h, -78.9 ± 2.83 mV; post Ni^{2+} V_h, -75.3 ± 5.52 mV; $n = 5$; $p > 0.05$). Together, these tests established the ability to interfere with Cav3–Kv4 function in both stellate and granule cells through internal dialysis of the PanKChIP antibody.

We thus used a PanKChIP antibody (1:100 dilution) to assess the effects of the Cav3–Kv4 complex in granule cells in response to square-wave current pulses (1 s; Fig. 4*A*). These *F–I* plots revealed a difference in the level of baseline excitability between granule cells in reporting a higher mean firing rate gain of 6.7 ± 0.32 Hz/pA ($n = 5$) in lobule 2 cells compared with 5.3 ± 0.49 Hz/pA ($n = 6$) in lobule 9 cells ($p < 0.05$). When the PanKChIP antibody was included in the electrode, it had no significant effect on the gain of lobule 2 cells from control conditions (Fig. 4). However, when the PanKChIP antibody was infused into lobule 9 cells, it significantly increased firing rate gain to 8.8 ± 0.57 Hz/pA ($n = 5$; $p < 0.001$), reflecting an ~65% increase in excitability that exceeded that of lobule 2 cells (Fig. 4*B*,*C*). In assessing the reasons for a selective increase in gain for lobule 9 cells, we found that it did not reflect a decrease in AHP amplitude ($n = 6$; $p > 0.05$) or spike threshold ($n = 6$; $p > 0.05$). We note that lobule 9 cells have a higher input resistance (R_i) than lobule 2 cells, as measured using hyperpolarizing current pulses (lobule 2 cells, 1.6 ± 0.18 GΩ, $n = 10$; lobule 9 cells, 2.4 ± 0.15 GΩ, $n = 15$; $p < 0.05$). This difference in R_i persisted in cells recorded with internal PanKChIP antibody (lobule 2 cells, 1.35 ± 0.05 GΩ, $n = 3$; lobule 9 cells, 2.15 ± 0.22 GΩ, $n = 3$; $p < 0.05$), indicating that the antibody did not differentially affect R_i. However, the native difference in R_i could contribute to a higher gain of firing in lobule 9 cells in the absence of a Cav3–Kv4 interaction. As indicated in Figure 1*C*, lobule 9 cells also have approximately four times the density of I_T compared with lobule 2 cells, which could

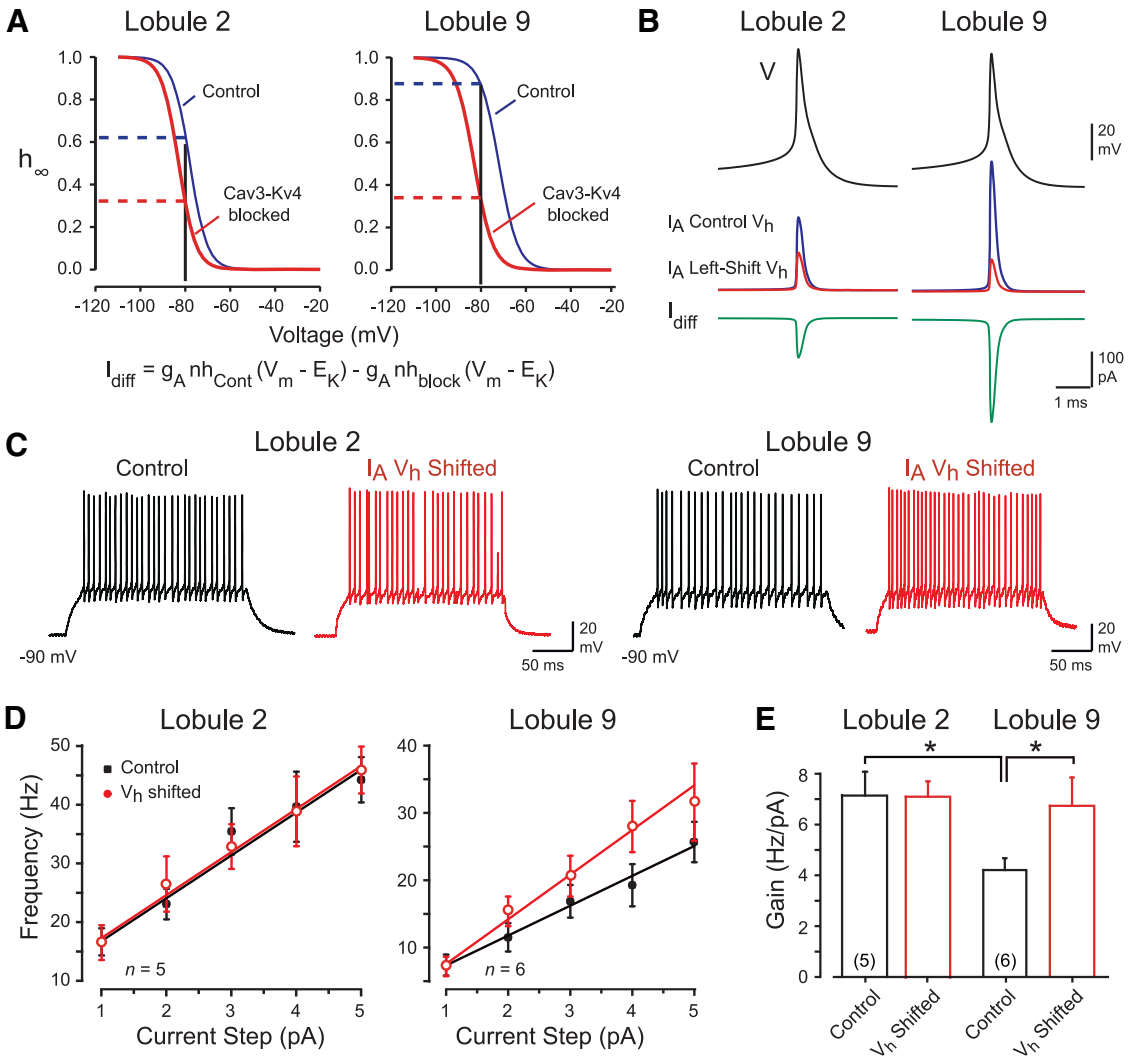

Figure 5. Dynamic clamp reveals that a shift in I_A V_h is sufficient to reproduce the effects of a Cav3–Kv4 interaction. ***A***, Inactivation curves of the I_A model show the difference in I_A availability before and after a left shift corresponding to the measured effect of blocking the Cav3–Kv4 complex in lobules 2 and 9 (see Fig. 2***C***). The predicted effect on I_A availability for a −80 mV holding potential is shown by dashed lines. ***B***, Examples of I_A predicted to be evoked by a spike response (*V*) for control conditions and after blocking the Cav3–Kv4 interaction. The net inward difference current (I_{diff}) to inject through dynamic clamp is shown in the bottom row. ***C***, Recordings of granule cell firing in response to an injected current pulse before and after applying a shift in I_A V_h under dynamic clamp according to the contribution of the Cav3–Kv4 interaction (as in ***A*** and ***B***). ***D***, ***E***, Frequency– current plots (***D***) and bar plots of the gain of firing (***E***) under control conditions and during dynamic clamp shifts in I_A V_h (as in ***A*** and ***B***). *$p < 0.05$, Student's paired *t* test.

increase spike firing to depolarizing current pulses when Cav3–Kv4 complex function is reduced by the antibody. Together, these results indicate that the excitability of lobule 9 cells in terms of firing rate gain would be substantially higher if not for the inhibitory influence of the Cav3–Kv4 complex.

Simulated shifts in I_A V_h through dynamic clamp increase the gain of lobule 9 cells

To further test the role of the Cav3–Kv4 complex in shaping firing rate gain, we used dynamic clamp. With this approach, we could test whether a selective shift in I_A V_h was sufficient to reproduce the effects of blocking the Cav3–Kv4 complex, but without the issues of selectivity inherent to pharmacological interventions. Biophysical parameters for I_A V_h before and after blocking the interaction (Fig. 1) were used to model the availability of I_A in granule cells with or without the influence of the Cav3–Kv4 complex. Examination of voltage-inactivation plots revealed that removing the Cav3–Kv4 influence in lobule 2 cells increased the extent of I_A inactivation at −80 mV from ~0.37 to ~0.69 (Fig. 5*A*, dashed lines). By comparison, when the Cav3–Kv4 complex was interrupted in lobule 9 cells, it increased I_A state of inactivation from ~0.13 to ~0.67 (Fig. 5*A*). These considerations allowed us to calculate the net inward or difference current (I_{diff}) to inject to simulate a reduction in I_A corresponding to a mean left shift in I_A V_h of −5.04 mV in lobule 2 cells and −10.5 mV in lobule 9 cells during a spike response (Fig. 5*B*). This is important in that we could assess the extent to which a modified I_A V_h brought about by the Cav3–Kv4 complex could account for the results obtained with PanKChIP antibody infusion in the absence of any pharmacological blockers.

In lobule 2 cells, we found that a dynamic shift of I_A V_h (−5.04 mV) produced no significant change in the gain of firing. In contrast, dynamically reducing I_A availability in lobule 9 cells with a shift in I_A V_h (−10.5 mV) induced ~60% increase in the gain of firing from 4.2 ± 0.46 to 6.7 ± 1.1 Hz/pA ($p < 0.05$; Fig. 5*C–E*). As found for direct current injection, there was no significant change in AHP amplitudes in either lobule during dynamic clamp (lobule 2, $n = 6$, $p > 0.05$; lobule 9, $n = 6$, $p > 0.05$). A

lower mean spike threshold was evident in lobule 2 but not lobule 9 cells (lobule 2, $n = 6$, $p < 0.01$), indicating that the increase in gain of firing in lobule 9 cells during dynamic clamp occurred independently of spike threshold. These results are important in revealing that shifts in I_A V_h that simulate the effects of the Cav3–Kv4 complex are sufficient to produce the same relative shift in gain of firing between lobule 2 and 9 granule cells as detected by interfering with Cav3–Kv4 function.

The Cav3–Kv4 complex differentially controls granule cell responses to MF input

Recordings made *in vivo* in the vermis of lobules 1 and 2 indicate that cells respond predominantly to lower-limb movements (Eccles et al., 1968; Valle et al., 2012), whereas those in lobules 9 and 10 respond to vestibular inputs (Arenz et al., 2008; Chadderton et al., 2014). These and other studies indicate two general patterns of MF input and granule cell output. The most common is a high-frequency burst of four to five MF spikes that generates a similar burst in granule cells (Chadderton et al., 2004; Rancz et al., 2007; Ekerot and Jörntell, 2008; Arenz et al., 2009). By comparison, granule cells in the caudal cerebellum must respond to gradual increases or decreases in the frequency of MF input (Arenz et al., 2008). We note that distinctions of this nature are not absolute, as MF input reflecting tonic or burst activity has been reported in either region (Barmack and Yakhnitsa, 2008; Chadderton et al., 2014). Nonetheless, we chose these two very different forms of input as representative cases to test the hypothesis that a differential expression of the Cav3–Kv4 complex serves to shape the postsynaptic response in a manner that promotes efficient transfer of MF burst or tonic inputs.

Simulated MF EPSCs

In determining the steps required to examine the role of the Cav3–Kv4 complex during MF-evoked synaptic activation, we found that perfusing 300 μM Ni^{2+} dramatically reduced the MF EPSC (Fig. 3*D*), preventing us from directly blocking Cav3 channels. We also sought to restrict analysis to postsynaptic mechanisms controlled by the Cav3–Kv4 complex in granule cells. We thus fit the MF-evoked EPSC with a sum of exponentials to create a simEPSC waveform that we reinjected as a postsynaptic stimulus to create a MF simulated EPSP (simEPSP; Fig. 3*E*). We then used internal dialysis of the PanKChIP antibody to interfere with the Cav3–Kv4 complex to determine its contribution to processing MF-evoked output. Two protocols were constructed with the simEPSC to produce a train of four EPSPs at 100 Hz or a repetitive series of simEPSCs introduced with a gradual oscillatory swing from 40–80 Hz to simulate two successive phases of slow shift in vestibular-like input. Excitatory and inhibitory synaptic transmission was also blocked to focus on postsynaptic mechanisms. The amplitude of the EPSC was fixed in all recordings to an initial peak of 20 pA.

MF burst input

We hypothesized that the relative lack of a Cav3–Kv4 interaction in lobule 2 cells would be more appropriate for processing a short-lived, high-frequency input as reported for granule cells responding to tactile stimuli *in vivo* (Chadderton et al., 2004). To assess this, we injected the train of four simEPSCs at 100 Hz into granule cells and measured the number of spikes fired. The shorter charging curve associated with simEPSC injection compared with square-wave pulses (see Materials and Methods) further allowed us to measure first-spike latency. The number of spikes evoked by the simEPSP burst in control conditions was

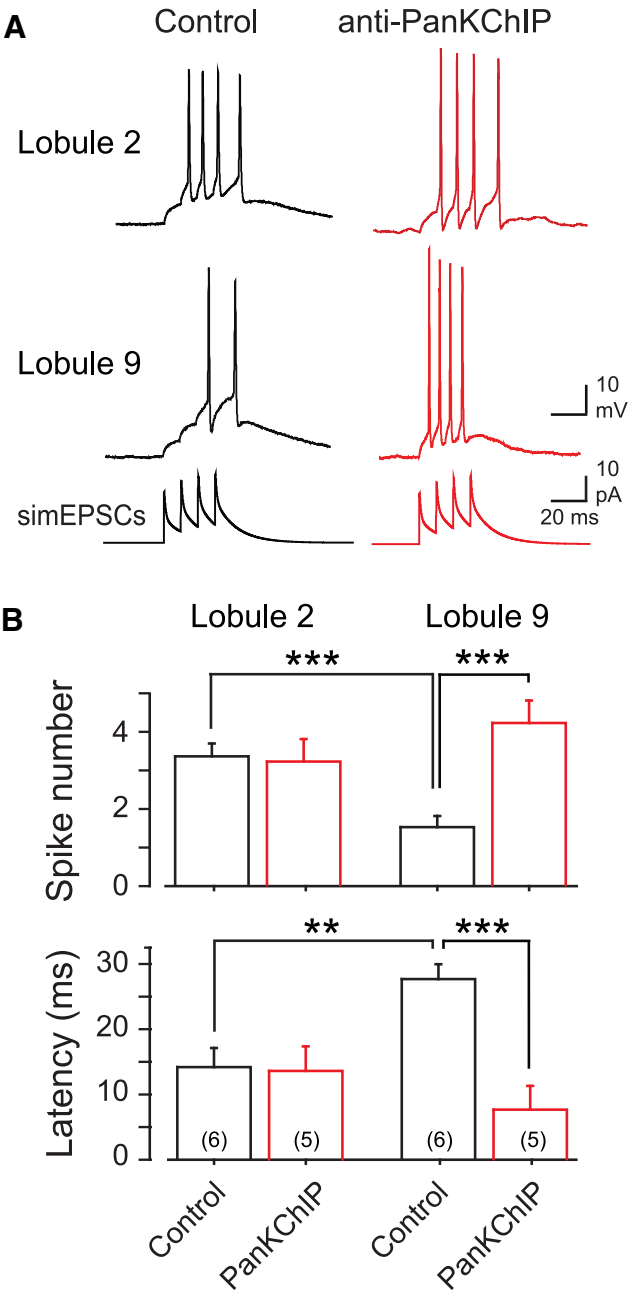

Figure 6. The Cav3–Kv4 complex selectively regulates the response of lobule 9 cells to bursts of synaptic input. ***A***, Recordings of the response of granule cells to a train of four simEPSCs (100 Hz) to simulate high-frequency inputs typical of tactile stimuli. Recordings are taken from different granule cells in the absence or presence of the internally perfused PanKChIP antibody (1:100 dilution) to block the Cav3–Kv4 interaction. Shown in the bottom row are the series of simEPSCs used to evoke simEPSPs. ***B***, Bar plots of the mean number of spikes and first spike latency in response to a four-pulse 100 Hz simEPSC train (as in ***A***) in the absence or presence of PanKChIP antibody in the electrode. Anti-PanKChIP invokes a selective increase in spike number and a decrease in first-spike latency in lobule 9 granule cells. Sample numbers for mean values are shown in parentheses. $^{**}p < 0.01$; $^{***}p < 0.001$, Student's unpaired *t* test.

significantly higher in lobule 2, with a mean of 3.3 ± 0.33 ($n = 6$) spikes compared with 1.3 ± 0.21 spikes in lobule 9 cells ($n = 6$; $p < 0.001$; Fig. 6). The infusion of the PanKChIP antibody in a separate population of cells had no significant effect on the number of spikes evoked in lobule 2 cells ($n = 5$; $p > 0.05$) but significantly increased spike output in lobule 9 cells from 1.3 spikes to 4.2 ± 0.58 ($n = 5$; $p < 0.001$). The latency to first spike was also significantly different between lobules under control

conditions, with a delay of 14 ± 3 ms (n = 6) in lobule 2 cells and 27 ± 2 ms (n = 6) in lobule 9 cells ($p < 0.01$; Fig. 6*B*). Infusion of the PanKChIP antibody in another population of cells resulted in a significantly shorter latency to first spike only in lobule 9 cells, reduced from 27 to 8 ± 3 ms (n = 5; $p < 0.001$; Fig. 6*B*). Thus, the relative lack of a Cav3–Kv4 influence in lobule 2 allows granule cells to respond more effectively than lobule 9 cells to a tactile-like stimulus by generating spikes at short latency and with a near one-to-one transference of a presynaptic spike burst to a granule cell spike burst.

MF vestibular-like input

To test the ability of a granule cell to follow a vestibular-like input, we injected the simEPSC stimulus that varied from 40 to 80 Hz with two cycles of oscillatory swing over 4 s (Fig. 7*A*). Under control conditions, lobule 2 cells began firing almost immediately after initiating the simEPSC train (EPSC frequency, 43 ± 1.3 Hz; n = 5) and rose rapidly in frequency during the first rise in EPSC input frequency (Fig. 7*B*). In three of five cells, spike discharge was maintained throughout most of the first and second period of the oscillation, with a temporary slowing of discharge frequency during the decrease in simEPSP frequency to 40 Hz (Fig. 7*B*). In two of five cells, spike firing on the second cycle of the oscillation was less reliable, with frequent failure of spike discharge as spike amplitude dropped below frequency-following capability. Average plots of spike amplitude revealed a progressive decline in amplitude during the first cycle of simEPSCs and a more precipitous drop during the second cycle of stimuli (Fig. 7*B*).

By comparison, presenting the same stimulus to lobule 9 cells evoked a much more stable response under control conditions. Lobule 9 cells responded with an initial delay in firing until the EPSC input frequency rose to 53 ± 3.3 Hz (n = 6) and then slowed in frequency (n = 2) or paused firing (n = 4) as input frequency slowed (Fig. 7*C*). Unlike lobule 2 cells, this pattern was then repeated without substantial variation on the second period of simEPSC stimuli. In the same manner, spike amplitude in lobule 9 cells was far more stable than lobule 2 cells, maintaining sufficient height to support reliable firing during both periods of the oscillatory input once input frequency threshold was attained (Fig. 7*C*).

We then compared these results to separate populations of cells in which the

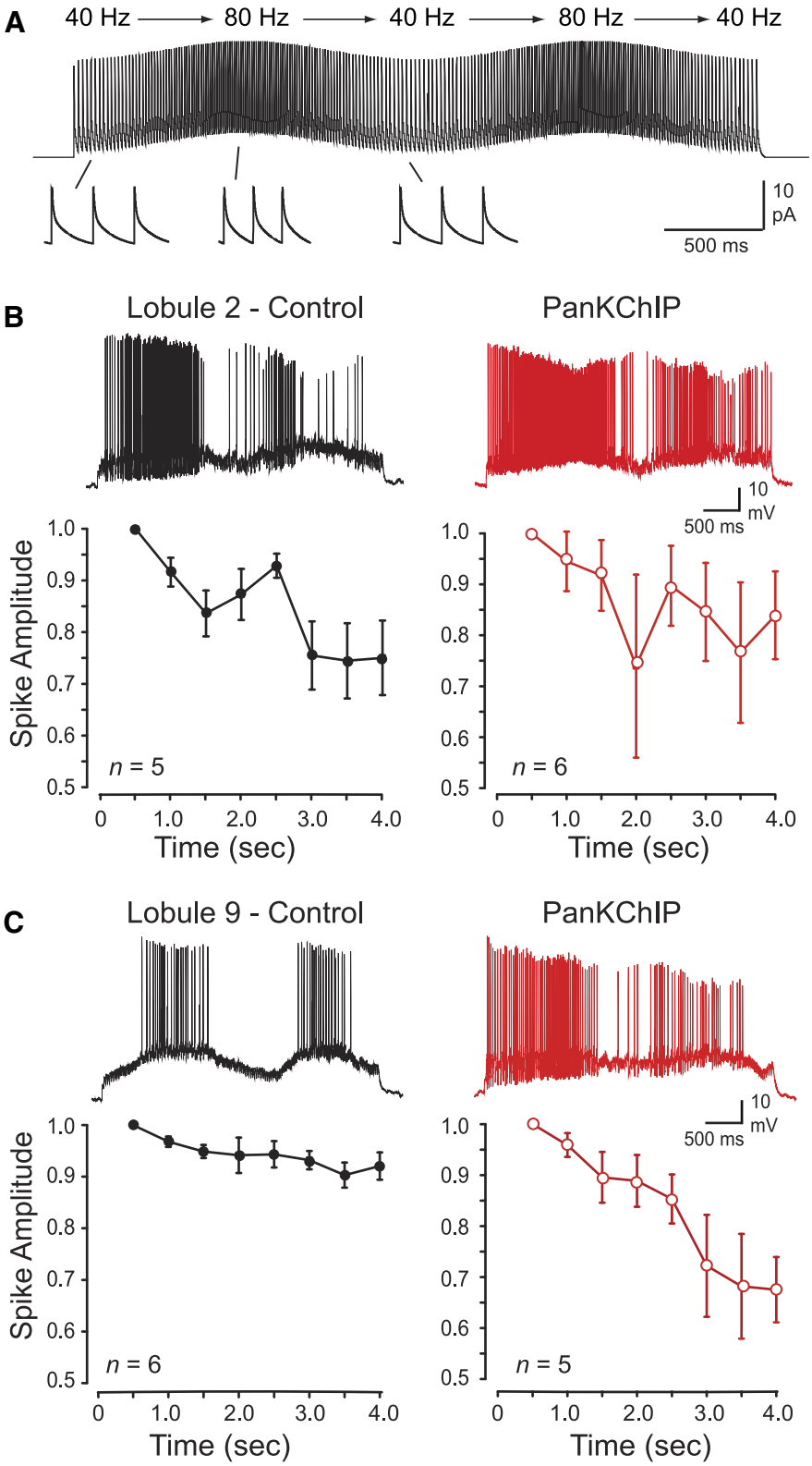

Figure 7. Spike discharge in lobule 9 granule cells is more capable of following MF simEPSPs delivered in a pattern simulating vestibular-like input. ***A***, Example of the train of MF simEPSCs with a pattern shifting in an oscillatory manner between 40 – 80 Hz. Single EPSCs are shown expanded (bottom). ***B***, ***C***, Recordings during two cycles of oscillatory simEPSP frequencies (as in ***A***) aligned with time points on the abscissa. Left, Spike amplitude in lobule 2 granule cells (***B***) fails progressively after a second rise in simEPSC frequency but is maintained in lobule 9 granule cells (***C***). Right, Separate populations of cells show that internal dialysis of a PanKChIP antibody (1:100 dilution) to block the Cav3–Kv4 interaction induces a greater decrease in spike amplitude and frequency-following capability in lobule 9 cells compared with lobule 2 cells. A 500 ms bin width was used to calculate mean spike amplitudes in ***B*** and ***C***.

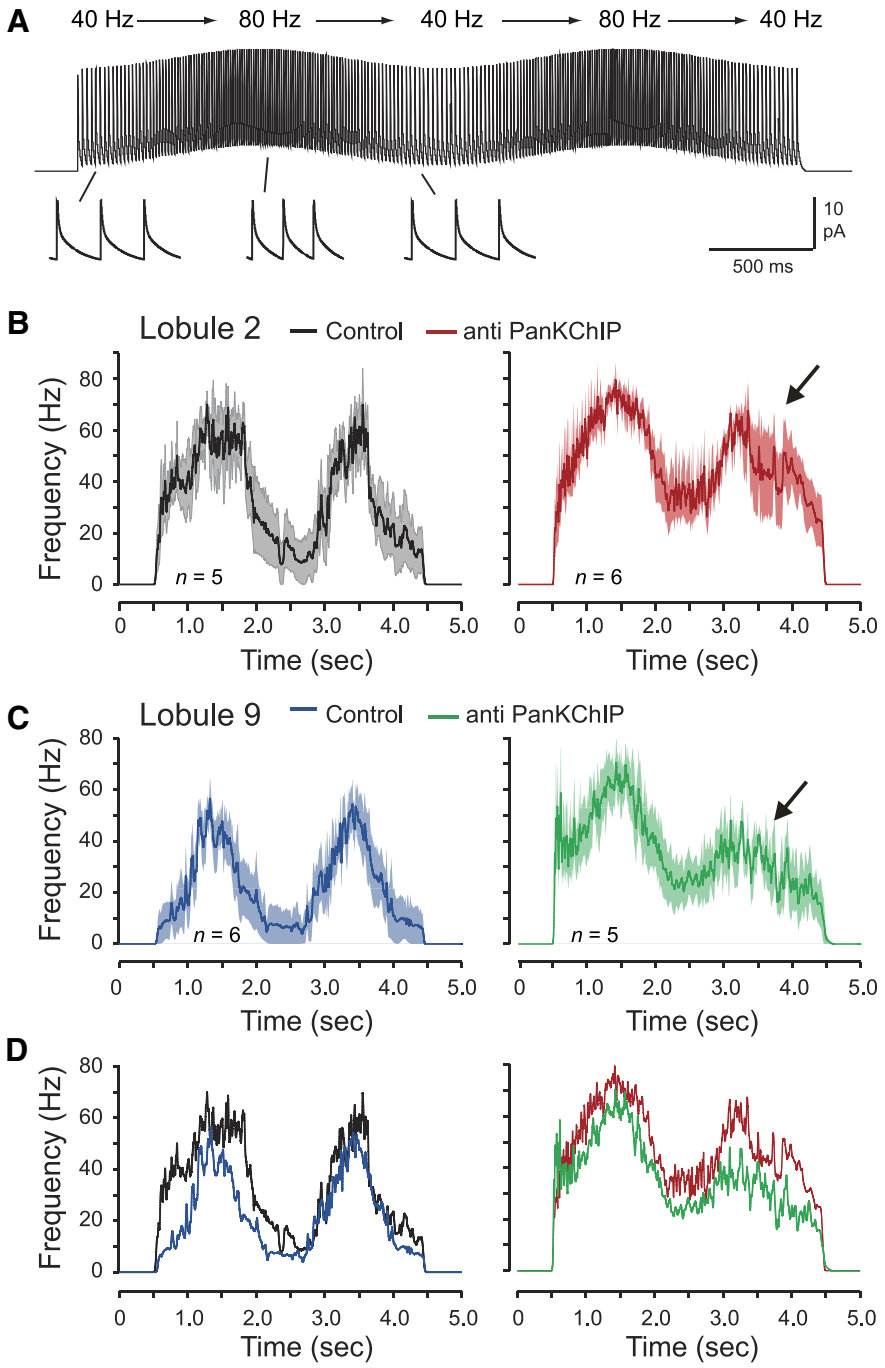

Figure 8. Granule cells in lobule 9 have greater frequency-following capability for EPSCs delivered in a pattern simulating vestibular-like input. ***A***, Example of the train of MF simEPSCs evoked by postsynaptic injection with a pattern shifting in an oscillatory manner between 40 and 80 Hz. Single EPSCs are shown expanded at the bottom. ***B–D***, Average spike-frequency plots over time of lobule 2 and 9 granule cells in response to the input shown in ***A***, with responses superimposed in ***D***. Left, Lobule 9 granule cells respond in a more graded manner and can better follow oscillatory simEPSC inputs compared with lobule 2 cells. Right, Dialyzing anti-PanKChIP (1:100 dilution) in the electrode to block the Cav3–Kv4 interaction converts the response of lobule 9 cells (***C***) to one closely resembling lobule 2 cells (***B***). Shaded areas in ***B*** and ***C*** reflect SEM.

PanKChIP antibody (1:100 dilution) was included in the electrode. In lobule 2 cells, interfering with Cav3–Kv4 function did not rescue the progressive failure in spike amplitude, with a continued decrease in amplitude through both cycles of the oscillatory input (Fig. 7*B*). In contrast, blocking Cav3–Kv4 function in lobule 9 cells resulted in a progressive loss of spike amplitude over both phases of oscillatory input, coming to essentially resemble the conditions found in lobule 2 cells under control conditions (Fig. 7*B*,*C*).

A separate analysis of spike frequency revealed that the Cav3–Kv4 interaction underlies a difference in frequency-following capability between lobule 2 and 9 cells. Under control conditions, lobule 2 cells exhibited a rapid increase in frequency to a mean of 67 ± 14.4 Hz ($n = 5$) by the peak of the first input cycle of simEPSCs and a decrease to peak frequency of 54 ± 8.1 Hz on the second cycle (Fig. 8*A*,*B*). Lobule 9 cells instead produced a graded response in spike discharge as simEPSCs gradually increased spike output to 46 ± 7.0 Hz ($n = 6$) by the peak of the first oscillatory phase (Fig. 8*C*). Spike output in lobule 9 cells then responded in an equivalent manner during the second phase of the oscillatory input and reached a similar peak frequency as the first oscillation (Fig. 8*C*).

Infusing the PanKChIP antibody to block the Cav3–Kv4 interaction had more of an effect on lobule 2 cells by enhancing the initial increase and peak in firing frequency and the lower limit of output frequency when EPSC stimuli returned to 40 Hz (Fig. 8*B*). In lobule 9 cells, infusion of the PanKChIP antibody essentially converted the pattern of spike output to that encountered in lobule 2 cells, with a rapid increase in firing to a higher peak frequency on the first phase of the oscillatory input and a pronounced reduction in frequency-following capability on the second phase of the oscillation (Fig. 8*C*,*D*).

Discussion

Signal processing in cerebellar cortex must contend with the fact that MF input conveys information from an enormous range of peripheral receptors that encode different sensory stimuli. One solution to address this is to compartmentalize MF input across cerebellar lobules, as reflected by the separation of tactile/joint information and vestibular inputs between cerebellar lobules 2 and 9. At the cellular level, a combination of presynaptic and postsynaptic mechanisms can further tune cell responsiveness to particular features of a stimulus. We know that MF inputs to granule cells exhibit different patterns of presynaptic spike discharge in relation to sensory information (Chadderton et al., 2004; Arenz et al., 2008; Barmack and Yakhnitsa, 2011). The density of UBCs are more prominent in posterior lobules (Mugnaini et al., 2011; Kim et al., 2012). The current study now reveals that the postsynaptic excitability of granule cells and their ability to process MF synaptic input is also differentially regulated across cerebellar lobules by the Cav3–Kv4 ion channel complex.

Expression pattern of Cav3–Kv4 complex subunits

The role of a Cav3–Kv4 complex was first described in cerebellar stellate cells, where Cav3-mediated calcium influx invokes an increase in I_A by selectively right-shifting Kv4 V_h (Molineux et al., 2005; Anderson et al., 2010a,b, 2013). To function the Cav3–Kv4 complex requires, at a minimum, any of the Cav3 or Kv4 channel isoforms together with the KChIP3 isoform of a calcium-sensing molecule (Anderson et al., 2010a,b). Since expression of these subunits varies on a regional basis (Serôdio and Rudy, 1998; Talley et al., 1999; Xiong et al., 2004; McKay et al., 2006; Amarillo et al., 2008; Clark et al., 2008), it is possible that a Cav3–Kv4 interaction may depend on the specific expression pattern of the responsible subunits. Cerebellar granule cells have been well characterized in terms of the expression of I_A, as governed by a Kv4 complex composed of Kv4 α-subunits and DPP and KChIP accessory proteins (Bardoni and Belluzzi, 1993; Serôdio and Rudy, 1998; Amarillo et al., 2008; Nadin and Pfaffinger, 2010; Jerng and Pfaffinger, 2012). Importantly, isoforms of each of these different subunits exhibit gradients of expression across lobules (Serôdio and Rudy, 1998; Talley et al., 1999; Xiong et al., 2004; Amarillo et al., 2008; Clark et al., 2008), providing the potential to influence the Cav3–Kv4 interaction. Yet under our recording conditions where calcium influx remained intact, we found no clear difference in the biophysical properties of I_A in granule cells of lobule 2 or 9 that might be expected to arise from these accessory subunits. Instead, blocking Cav3 channel calcium influx revealed a Cav3–Kv4 interaction that was most effective in modulating spike output in lobule 9 cells, indicating a baseline calcium-dependent modulation of Kv4 function between lobules.

The current study is the first to report an expression of the Cav3 calcium current in granule cells, with an approximate four times higher density in lobule 9 compared with cells in lobule 2. This is important because Cav3 channels are the only identified source of voltage-gated calcium influx we have so far found capable of modifying the voltage dependence of Kv4 channel inactivation (Anderson et al., 2010a,b). Indeed, several tests support the importance of Cav3 channel expression in governing Cav3–Kv4 function across cerebellar lobules. A higher level of T-type current in lobule 9 cells matches well with reports of a high level of Cav3.1 mRNA in granule cells of lobules 6–10 compared with only a weak and uniform expression of Cav3.3 mRNA across all lobules (Talley et al., 1999). The V_h of I_A was more positively shifted in lobule 9 cells compared with lobule 2 cells in control conditions, and blocking Cav3 channel conductance produced a selective shift in Kv4 V_h that was greater in magnitude in lobule 9 versus lobule 2 cells. Once Cav3 channel conductance was blocked, the value of Kv4 V_h and I_A density between cells in each lobule was not significantly different. The ability to selectively modify spike output in lobule 9 cells by interfering with the Cav3–Kv4 complex or by dynamically shifting Kv4 V_h lends additional support for the role of the Cav3–Kv4 complex in lobule 9 granule cells.

Function of the Cav3–Kv4 complex

Interestingly, the role of Kv4 channels in controlling spike output in granule cells has not been extensively analyzed. One report by D'Angelo et al. (1998) using 2 mM 4-AP indicated that a full block of at least Kv4 channels reduced the AHP and first-spike latency and, in some cases, shifted spike output from tonic firing to an irregular burst mode. Although 4-AP will also block other voltage-gated potassium channels (Bardoni and Belluzzi, 1993), these results are interesting in suggesting that Kv4 channels may act to regulate the interspike interval and enable tonic firing of granule cells. The Cav3–Kv4 complex would then function to adjust the gain of a linear input–output function according to modulation of Kv4 V_h. The current work also indicates that the Cav3–Kv4 complex ordinarily serves to reduce the gain of firing in lobule 9 granule cells compared with lobule 2 cells. Thus, without the influence of the Cav3–Kv4 complex, the gain of lobule 9 cells would be higher than that of lobule 2, revealing a basic difference in excitability that is regulated by Cav3 channel expression and its interaction with Kv4 channels.

The current work also establishes that the depolarization provided by MF EPSPs is sufficient to activate the Cav3 calcium influx required to modulate A-current availability and granule cell responsiveness. To test the effects of the Cav3–Kv4 complex on signal processing, we delivered two extremes of predicted MF input patterns. These tests showed that the ability for lobule 9 cells to follow a high-frequency burst of MF simEPSPs was muted compared with lobule 2 cells because of a greater inhibitory influence by the Cav3–Kv4 complex. Conversely, lobule 9 cells responded to oscillatory swings of simEPSP frequencies with a more graded and reproducible spike output over successive cycles of input than lobule 2 cells. Blocking the Cav3–Kv4 complex then converted the response capability of lobule 9 cells to that recorded in lobule 2 cells. The Cav3–Kv4 complex is thus well suited to shaping granule cell postsynaptic responses to the gradual frequency shifts of MF input inherent to vestibular inputs in caudal lobules. Conversely, a greatly reduced Cav3–Kv4 interaction in lobule 2 cells is conducive to allowing granule cells to respond quickly to MF burst input characteristic of tactile sensory input in anterior lobules. We note that our data set was obtained under conditions where inhibition was blocked and injection of simEPSCs was used to isolate postsynaptic effects of the Cav3–Kv4 complex. Therefore, it is expected that a differential expression of presynaptic or inhibitory mechanisms or synaptic plasticity between cerebellar lobules could further modify the response of granule cells to MF inputs.

Several theories have been put forth to account for signal processing by granule cells, including the "time window" hypothesis (D'Angelo and De Zeeuw, 2009), the detonator model (Rancz et al., 2007), and the coincidence detector model (Dean et al., 2010). It is intriguing that the time window and detonator models were based on data recorded from granule cells in Crus 1 and 2a (which receive whisker signals) and the coincidence detector model from data recorded in the C3 zone of anterior paravermis (which receives forelimb sensory signals), as discussed by Arenz et al. (2009). The contrasting theories then might simply reflect the different regions of the cerebellum on which they were based and relevant to signal processing for specific MF projections and the sensory input they convey. The reliance of the Cav3–Kv4 complex for Cav3 channel-mediated calcium influx seen here suggests that it will serve to modify MF input primarily in lobules 6–10 where Cav3.1 mRNA expression is high compared with anterior lobules. Comparing the activity of this complex and its relationship to existing theories of cerebellar signal processing between other lobules and outside the vermis region (i.e., Crus 1 and 2) awaits further analysis.

It is important to note that the channel subunits and accessory proteins that comprise the Cav3–Kv4 complex are differentially expressed across multiple brain structures. Achieving a functional Cav3–Kv4 complex may then also vary depending on the expression pattern of the underlying subunits elsewhere. For instance, in the hippocampus, several isoforms of the subunits that comprise a Cav3–Kv4 complex are differentially ex-

pressed between pyramidal cell populations (Xiong et al., 2004; McKay et al., 2006; Menegola and Trimmer, 2006). These results are interesting in suggesting that the Cav3–Kv4 complex may differentially regulate excitability across other neuronal populations according to the pattern of responsible subunits.

References

Amarillo Y, De Santiago-Castillo JA, Dougherty K, Maffie J, Kwon E, Covarrubias M, Rudy B (2008) Ternary Kv4.2 channels recapitulate voltage-dependent inactivation kinetics of A-type K+ channels in cerebellar granule neurons. J Physiol 586:2093–2106. CrossRef Medline

An WF, Bowlby MR, Betty M, Cao J, Ling HP, Mendoza G, Hinson JW, Mattsson KI, Strassle BW, Trimmer JS, Rhodes KJ (2000) Modulation of A-type potassium channels by a family of calcium sensors. Nature 403: 553–556. CrossRef Medline

Anderson D, Mehaffey WH, Iftinca M, Rehak R, Engbers JD, Hameed S, Zamponi GW, Turner RW (2010a) Regulation of neuronal activity by Cav3-Kv4 channel signaling complexes. Nat Neurosci 13:333–337. CrossRef Medline

Anderson D, Rehak R, Hameed S, Mehaffey WH, Zamponi GW, Turner RW (2010b) Regulation of the KV4.2 complex by CaV3.1 calcium channels. Channels (Austin) 4:163–167. CrossRef Medline

Anderson D, Engbers JD, Heath NC, Bartoletti TM, Mehaffey WH, Zamponi GW, Turner RW (2013) The Cav3–Kv4 complex acts as a calcium sensor to maintain inhibitory charge transfer during extracellular calcium fluctuations. J Neurosci 33:7811–7824. CrossRef Medline

Arenz A, Silver RA, Schaefer AT, Margrie TW (2008) The contribution of single synapses to sensory representation in vivo. Science 321:977–980. CrossRef Medline

Arenz A, Bracey EF, Margrie TW (2009) Sensory representations in cerebellar granule cells. Curr Opin Neurobiol 19:445–451. CrossRef Medline

Armstrong DM, Apps R, Marple-Horvat DE (1997) Aspects of cerebellar function in relation to locomotor movements. Prog Brain Res 114:401–421. CrossRef Medline

Bardoni R, Belluzzi O (1993) Kinetic study and numerical reconstruction of A-type current in granule cells of rat cerebellar slices. J Neurophysiol 69:2222–2231. Medline

Barmack NH, Yakhnitsa V (2008) Functions of interneurons in mouse cerebellum. J Neurosci 28:1140–1152. CrossRef Medline

Barmack NH, Yakhnitsa V (2011) Topsy turvy: functions of climbing and mossy fibers in the vestibulo-cerebellum. Neuroscientist 17:221–236. CrossRef Medline

Bengtsson F, Jörntell H (2009) Sensory transmission in cerebellar granule cells relies on similarly coded mossy fiber inputs. Proc Natl Acad Sci U S A 106:2389–2394. CrossRef Medline

Carrasquillo Y, Burkhalter A, Nerbonne JM (2012) A-type K+ channels encoded by Kv4.2, Kv4.3 and Kv1.4 differentially regulate intrinsic excitability of cortical pyramidal neurons. J Physiol 590:3877–3890. CrossRef Medline

Chadderton P, Margrie TW, Häusser M (2004) Integration of quanta in cerebellar granule cells during sensory processing. Nature 428:856–860. CrossRef Medline

Chadderton P, Schaefer AT, Williams SR, Margrie TW (2014) Sensory-evoked synaptic integration in cerebellar and cerebral cortical neurons. Nat Rev Neurosci 15:71–83. CrossRef Medline

Clark BD, Kwon E, Maffie J, Jeong HY, Nadal M, Strop P, Rudy B (2008) DPP6 localization in brain supports function as a Kv4 channel associated protein. Front Mol Neurosci 1(8):1–11. CrossRef Medline

Connor JA, Stevens CF (1971) Prediction of repetitive firing behaviour from voltage clamp data on an isolated neurone soma. J Physiol 213:31–53. Medline

Cull-Candy SG, Marshall CG, Ogden D (1989) Voltage-activated membrane currents in rat cerebellar granule neurones. J Physiol 414:179–199. Medline

D'Angelo E, De Zeeuw CI (2009) Timing and plasticity in the cerebellum: focus on the granular layer. Trends Neurosci 32:30–40. CrossRef Medline

D'Angelo E, De Filippi G, Rossi P, Taglietti V (1997) Synaptic activation of Ca2+ action potentials in immature rat cerebellar granule cells in situ. J Neurophysiol 78:1631–1642. Medline

D'Angelo E, De Filippi G, Rossi P, Taglietti V (1998) Ionic mechanism of electroresponsiveness in cerebellar granule cells implicates the action of a persistent sodium current. J Neurophysiol 80:493–503. Medline

Dean P, Porrill J, Ekerot CF, Jörntell H (2010) The cerebellar microcircuit as an adaptive filter: experimental and computational evidence. Nat Rev Neurosci 11:30–43. CrossRef Medline

Diana MA, Otsu Y, Maton G, Collin T, Chat M, Dieudonné S (2007) T-type and L-type Ca^{2+} conductances define and encode the bimodal firing pattern of vestibulocerebellar unipolar brush cells. J Neurosci 27:3823–3838. CrossRef Medline

Dorval AD, Christini DJ, White JA (2001) Real-time linux dynamic clamp: a fast and flexible way to construct virtual ion channels in living cells. Ann Biomed Eng 29:897–907. CrossRef Medline

Eccles JC, Provini L, Strata P, Táboríková H (1968) Analysis of electrical potentials evoked in the cerebellar anterior lobe by stimulation of hindlimb and forelimb nerves. Exp Brain Res 6:171–194. CrossRef Medline

Ekerot CF, Jörntell H (2008) Synaptic integration in cerebellar granule cells. Cerebellum 7:539–541. CrossRef Medline

Ellinor PT, Zhang JF, Randall AD, Zhou M, Schwarz TL, Tsien RW, Horne WA (1993) Functional expression of a rapidly inactivating neuronal calcium channel. Nature 363:455–458. CrossRef Medline

Engbers JD, Anderson D, Asmara H, Rehak R, Mehaffey WH, Hameed S, McKay BE, Kruskic M, Zamponi GW, Turner RW (2012) Intermediate conductance calcium-activated potassium channels modulate summation of parallel fiber input in cerebellar Purkinje cells. Proc Natl Acad Sci U S A 109:2601–2606. CrossRef Medline

Gall D, Prestori F, Sola E, D'Errico A, Roussel C, Forti L, Rossi P, D'Angelo E (2005) Intracellular calcium regulation by burst discharge determines bidirectional long-term synaptic plasticity at the cerebellum input stage. J Neurosci 25:4813–4822. CrossRef Medline

Glickstein M, Sultan F, Voogd J (2011) Functional localization in the cerebellum. Cortex 47:59–80. CrossRef Medline

Iftinca M, McKay BE, Snutch TP, McRory JE, Turner RW, Zamponi GW (2006) Temperature dependence of T-type calcium channel gating. Neuroscience 142:1031–1042. CrossRef Medline

Jerng HH, Pfaffinger PJ (2012) Incorporation of DPP6a and DPP6K variants in ternary Kv4 channel complex reconstitutes properties of A-type K current in rat cerebellar granule cells. PLoS One 7:e38205. CrossRef Medline

Jerng HH, Pfaffinger PJ, Covarrubias M (2004) Molecular physiology and modulation of somatodendritic A-type potassium channels. Mol Cell Neurosci 27:343–369. CrossRef Medline

Jerng HH, Kunjilwar K, Pfaffinger PJ (2005) Multiprotein assembly of Kv4.2, KChIP3 and DPP10 produces ternary channel complexes with ISA-like properties. J Physiol 568:767–788. CrossRef Medline

Kim JA, Sekerková G, Mugnaini E, Martina M (2012) Electrophysiological, morphological, and topological properties of two histochemically distinct subpopulations of cerebellar unipolar brush cells. Cerebellum 11:1012–1025. CrossRef Medline

Kunjilwar K, Qian Y, Pfaffinger PJ (2013) Functional stoichiometry underlying KChIP regulation of Kv4.2 functional expression. J Neurochem 126: 462–472. CrossRef Medline

Lee JH, Gomora JC, Cribbs LL, Perez-Reyes E (1999) Nickel block of three cloned T-type calcium channels: low concentrations selectively block alpha1H. Biophys J 77:3034–3042. CrossRef Medline

Liss B, Franz O, Sewing S, Bruns R, Neuhoff H, Roeper J (2001) Tuning pacemaker frequency of individual dopaminergic neurons by Kv4.3L and KChip3.1 transcription. EMBO J 20:5715–5724. CrossRef Medline

Locatelli F, Bottà L, Prestori F, Masetto S, D'Angelo E (2013) Late-onset bursts evoked by mossy fibre bundle stimulation in unipolar brush cells: evidence for the involvement of H-and TRP-currents. J Physiol 591:899–918. CrossRef Medline

Maffie J, Rudy B (2008) Weighing the evidence for a ternary protein complex mediating A-type K+ currents in neurons. J Physiol 586:5609–5623. CrossRef Medline

McKay BE, McRory JE, Molineux ML, Hamid J, Snutch TP, Zamponi GW, Turner RW (2006) Ca(V)3 T-type calcium channel isoforms differentially distribute to somatic and dendritic compartments in rat central neurons. Eur J Neurosci 24:2581–2594. CrossRef Medline

Menegola M, Trimmer JS (2006) Unanticipated region- and cell-specific downregulation of individual KChIP auxiliary subunit isotypes in Kv4.2 knock-out mouse brain. J Neurosci 26:12137–12142. CrossRef Medline

Molineux ML, Fernandez FR, Mehaffey WH, Turner RW (2005) A-type and

T-type currents interact to produce a novel spike latency–voltage relationship in cerebellar stellate cells. J Neurosci 25:10863–10873. CrossRef Medline

Mugnaini E, Sekerková G, Martina M (2011) The unipolar brush cell: a remarkable neuron finally receiving deserved attention. Brain Res Rev 66:220–245. CrossRef Medline

Nadin BM, Pfaffinger PJ (2010) Dipeptidyl peptidase-like protein 6 is required for normal electrophysiological properties of cerebellar granule cells. J Neurosci 30:8551–8565. CrossRef Medline

Nadin BM, Pfaffinger PJ (2013) A new TASK for dipeptidyl peptidase-like protein 6. PLoS One 8:e60831. CrossRef Medline

Norris AJ, Foeger NC, Nerbonne JM (2010) Neuronal voltage-gated K+ (Kv) channels function in macromolecular complexes. Neurosci Lett 486: 73–77. CrossRef Medline

Rancz EA, Ishikawa T, Duguid I, Chadderton P, Mahon S, Häusser M (2007) High-fidelity transmission of sensory information by single cerebellar mossy fibre boutons. Nature 450:1245–1248. CrossRef Medline

Randall A, Tsien RW (1995) Pharmacological dissection of multiple types of Ca^{2+} channel currents in rat cerebellar granule neurons. J Neurosci 15: 2995–3012. Medline

Randall AD, Tsien RW (1997) Contrasting biophysical and pharmacological properties of T-type and R-type calcium channels. Neuropharmacology 36:879–893. CrossRef Medline

Rossi P, D'Angelo E, Magistretti J, Toselli M, Taglietti V (1994) Age-dependent expression of high-voltage activated calcium currents during cerebellar granule cell development in situ. Pflugers Arch 429:107–116. CrossRef Medline

Serôdio P, Rudy B (1998) Differential expression of Kv4 K+ channel subunits mediating subthreshold transient K+ (A-type) currents in rat brain. J Neurophysiol 79:1081–1091. Medline

Sillitoe RV, Joyner AL (2007) Morphology, molecular codes, and circuitry produce the three-dimensional complexity of the cerebellum. Annu Rev Cell Dev Biol 23:549–577. CrossRef Medline

Song WJ, Tkatch T, Baranauskas G, Ichinohe N, Kitai ST, Surmeier DJ (1998) Somatodendritic depolarization-activated potassium currents in rat neostriatal cholinergic interneurons are predominantly of the A type and attributable to coexpression of Kv4.2 and Kv4.1 subunits. J Neurosci 18:3124–3137. Medline

Talley EM, Cribbs LL, Lee JH, Daud A, Perez-Reyes E, Bayliss DA (1999) Differential distribution of three members of a gene family encoding low voltage-activated (T-type) calcium channels. J Neurosci 19:1895–1911. Medline

Tottene A, Moretti A, Pietrobon D (1996) Functional diversity of P-type and R-type calcium channels in rat cerebellar neurons. J Neurosci 16: 6353–6363. Medline

Tottene A, Volsen S, Pietrobon D (2000) Alpha(1E) subunits form the pore of three cerebellar R-type calcium channels with different pharmacological and permeation properties. J Neurosci 20:171–178. Medline

Valle MS, Eian J, Bosco G, Poppele RE (2012) The organization of cortical activity in the anterior lobe of the cat cerebellum during hindlimb stepping. Exp Brain Res 216:349–365. CrossRef Medline

Wang K, Lin MT, Adelman JP, Maylie J (2014) Distinct Ca(2+) sources in dendritic spines of hippocampal CA1 neurons couple to SK and Kv4 channels. Neuron 81:379–387. CrossRef Medline

Xiong H, Kovacs I, Zhang Z (2004) Differential distribution of KChIPs mRNAs in adult mouse brain. Brain Res Mol Brain Res 128:103–111. CrossRef Medline

Yuan W, Burkhalter A, Nerbonne JM (2005) Functional role of the fast transient outward K^+ current IA in pyramidal neurons in (rat) primary visual cortex. J Neurosci 25:9185–9194. CrossRef Medline

Zamponi GW, Bourinet E, Snutch TP (1996) Nickel block of a family of neuronal calcium channels: subtype- and subunit-dependent action at multiple sites. J Membr Biol 151:77–90. CrossRef Medline

Zhang JF, Randall AD, Ellinor PT, Horne WA, Sather WA, Tanabe T, Schwarz TL, Tsien RW (1993) Distinctive pharmacology and kinetics of cloned neuronal Ca2+ channels and their possible counterparts in mammalian CNS neurons. Neuropharmacology 32:1075–1088. CrossRef Medline